THE JOURNAL OF PHYSICAL CHEMISTRY B

Article

pubs.acs.org/JPCB

Effect of Temperature on Photophysical Properties of Polymeric Nanofiber Materials with Porphyrin Photosensitizers

Jan Suchánek,[†,‡] Petr Henke,[§] Jiří Mosinger,[§,⊥] Zdeněk Zelinger,[†] and Pavel Kubát*[,†]

[†]J. Heyrovský Institute of Physical Chemistry, v.v.i., Academy of Sciences of the Czech Republic, Dolejškova 3, 18223 Praha 8, Czech Republic

[‡]Faculty of Safety Engineering, Technical University of Ostrava, Lumírova 13, Ostrava-Vyškovice, 700 30 Ostrava, Czech Republic

[§]Faculty of Science, Charles University in Prague, Hlavova 2030, 128 43 Praha 2, Czech Republic

[⊥]Institute of Inorganic Chemistry, v.v.i., Academy of Sciences of the Czech Republic, 250 68 Řež, Czech Republic

Supporting Information

ABSTRACT: Electrospun nanofibers possess large surface to volume ratios, high porosity, and good mechanical properties that are necessary for biological applications. We prepared different types of photoactive polymeric nanofiber materials with encapsulated or externally bound porphyrin photosensitizers. The kinetics of formation and the decay of both singlet oxygen $O_2(^1\Delta_g)$ and porphyrin triplet states that are generated by irradiation of nanofiber materials in an air atmosphere or in an air-saturated aqueous solution were measured and evaluated by luminescence and transient absorption spectroscopy in the temperature range between 5 and 60 °C. We found shortening of the $O_2(^1\Delta_g)$ lifetime and a significant increase in singlet oxygen-sensitized delayed fluorescence at higher temperatures. These photophysical data show an increase in the diffusion coefficient for $O_2(^1\Delta_g)$ with temperature, and they are consistent with a stronger antibacterial effect of the nanofiber material on *Escherichia coli* at higher temperature.

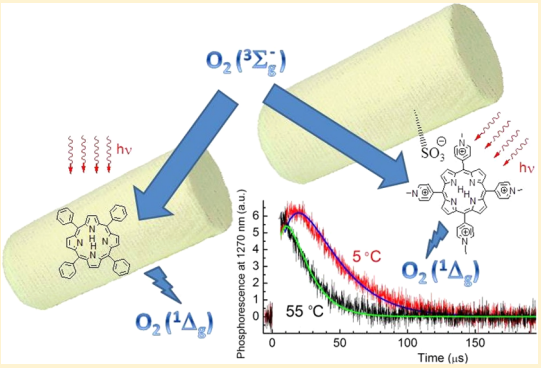

INTRODUCTION

The photosensitized production of singlet oxygen $O_2(^1\Delta_g)$ mediates the oxidative degradation of many molecules, and is important in several areas of biology and medicine,[1,2] including antibacterial treatment.[3] Recently, research efforts have been extended toward the design of novel hybrid materials in which photosensitizers are fixed to a solid support (e.g., polymers,[4,5] silica,[6] or glass[7]). This approach combines high efficiency in killing bacteria and viruses with a simple application.

In previous papers, we prepared different types of polymeric nanofiber materials with encapsulated[8,9] or externally bound[10] porphyrin/phthalocyanine photosensitizers that produce $O_2(^1\Delta_g)$ upon irradiation by visible light and exhibit antibacterial properties. The electrospun nanofibers possess large surface to volume ratios, increased porosity, and good mechanical properties for photobiological applications.[11] The polymeric architecture provides a functional nanoenvironment to alter the photophysical behavior of photosensitizers that affect photoreaction activity and selectivity. The small diameters of the nanofibers allow for the diffusion of $O_2(^1\Delta_g)$ outside of the fibers, where biological targets can be photooxidized, e.g., cell membranes[12] or proteins inside the cells.[13] Such nanomaterials are suitable for fabrication of filters for water disinfection[14] or wound dressings to combat infection.[15]

An important parameter to control the photooxidation efficiency and antibacterial properties of materials is the temperature. Singlet oxygen $O_2(^1\Delta_g)$ is likely a powerful oxidant at low temperature in ice/snow,[16] as concentrations of $O_2(^1\Delta_g)$ on illuminated ice can be much higher than in identical (but unfrozen) illuminated liquid solutions.[17]

We also expected that the photooxidation and/or antibacterial efficiency of nanofiber materials are influenced by temperature-dependent changes in photophysical parameters of the photosensitizer and the properties of its environment. It is known that the solvent-dependent channel for nonradiative deactivation of $O_2(^1\Delta_g)$ is dependent on temperature in a number of common solvents, yielding apparent activation energies of 1.2 kJ mol^{-1} for H_2O and 5.3 kJ mol^{-1} for D_2O.[18] The thermally activated process is also the diffusion of oxygen in polymers, with an expression analogous to the Arrhenius equation over a limited range of temperatures.[19]

This paper reports on the influence of temperature on the generation and decay of $O_2(^1\Delta_g)$ by porphyrin photosensitizers encapsulated inside or bound to polystyrene (PS) nanofiber materials. PS is a biocompatible polymer that is used

Received: March 26, 2014
Revised: April 29, 2014
Published: May 14, 2014

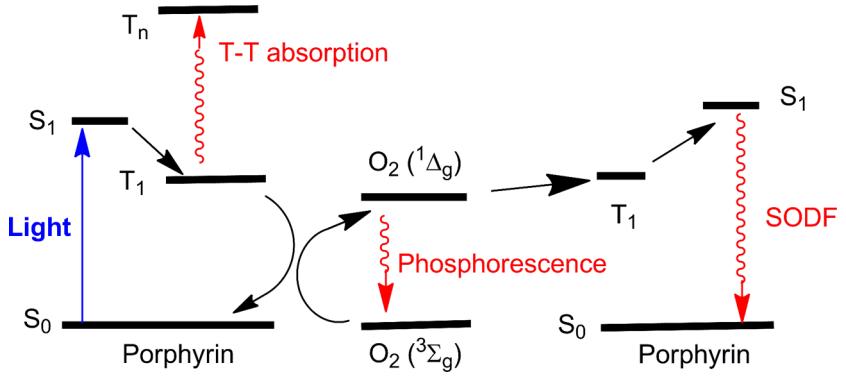

Figure 1. Simplified energy level diagram with T-T absorption, phosphorescence of $O_2(^1\Delta_g)$, and SODF produced by two porphyrin molecules and one oxygen molecule (all radiation processes used for monitoring of porphyrin triplet states and $O_2(^1\Delta_g)$ are displayed in red color).

extensively in cell culture experimentation.[20] Singlet oxygen $O_2(^1\Delta_g)$ was monitored by using its weak phosphorescence at ~1270 nm, and triplet porphyrins were monitored by transient absorption spectroscopy (T-T absorption, Figure 1). We also measured singlet oxygen-sensitized delayed fluorescence (SODF), which is an alternative and sensitive way to monitor both triplet porphyrin and $O_2(^1\Delta_g)$. Strong SODF signals occur via the reaction of triplet porphyrin photosensitizers with $O_2(^1\Delta_g)$. The results were compared with the photoantibacterial efficiency of the nanofiber materials at three different temperatures. This testing was performed on bacterial colonies of *Escherichia coli*.

MATERIALS AND METHODS

Chemicals. The following chemicals were purchased from Sigma-Aldrich and used as received: 5,10,15,20-tetraphenylporphyrin (TPP); 5,10,15,20-tetrakis(1-methylpyridinium-4-yl) porphyrin tetra (*p*-toluenesulfonate) (TMPyP); 5,10,15,20-tetrakis(4-sulfonatophenyl) porphyrin tetrasodium salt (TPPS); D_2O (99.9%); chlorosulfonic acid (HSO_3Cl); tetraethylamonium bromide (TEAB); cyclohexanone; *N*,*N*-dimethylformamide (DMF); agar; and LB medium. Phosphate buffered saline (PBS) was purchased from Lonza (Belgium). Commercial-grade PS (Krasten 137) was purchased from Synthos Kralupy a.s., Czech Republic. Larithane LS 1086 is an aliphatic elastomer based on linear polycarbonated diol, isophorone diisocyanate and extended isophorone diamine and was purchased from Novotex, Italy. Tecophilic HP-60D-60 is a thermoplastic elastomer consisting of segmented block copolymers and synthesized from diisocyanato-dicyclohexylmethane, 1,4-butanediol, and poly(ethylene glycol) and was purchased from Lubrizol Advanced Materials (USA).

Preparation of Nanofiber Materials. Nanofiber materials with encapsulated porphyrin were produced using the Nanospider electrospinning technology described in detail in a previous paper.[8] Typically, a mixture of porphyrins and polymers dissolved in solvent was used for electrospinning. The electrospun materials were produced in the form of thin membranes (thickness ~0.03 mm) on a polypropylene supporting textile. Before additional treatment and/or measurements, the textile was peeled off, and samples were fixed to a quartz plate. Preparation of nanofiber material with externally bound TMPyP is described in detail in a previous paper.[10] Briefly, PS nanofiber materials were prepared by electrospinning a mixture of 0.31 wt % TEAB and 99.69 wt % polystyrene dissolved in cyclohexanone. The material was sulfonated by chlorosulfonic acid at 10−12 °C. Finally, it was washed with deionized water until the pH reached a value of 6−7, and it was stored in water. The sulfonated nanofiber material (IEC = 4 mmol g^{-1}) was used as a substrate for the adsorption of the cationic photosensitizer TMPyP. The samples with a TMPyP/SO_3^- ratio of 7.5×10^{-3} were used for the experiments.

Properties of Nanofiber Materials. The morphology of the nanofiber materials was analyzed with a scanning electron microscope (SEM, FEI Quanta 200 with an Everhart-Thornley secondary electron detector). The thickness of the nanofibers was estimated using NIS Elements 4.0 image analysis software (Laboratory Imaging, Czech Republic). The UV/vis absorption spectra were recorded on a Cary 4000 UV−vis (Agilent) spectrometer equipped with an integration sphere. A sample of nanofiber material on a quartz plate was placed at the entrance to the sphere and measured in diffuse transmittance mode to minimize light scattering.

Photophysical Measurements. The measurements were performed in a 10 mm quartz cell placed inside a thermostatically controlled holder that was heated or cooled using the Peltier effect to maintain temperature stability to within 0.1 °C. A piece of the nanofiber material was placed on a quartz plate and inserted in a quartz cell with water or in the air atmosphere. For measurement in oxygen free condition, the samples were saturated by argon or evacuated. The total pressure in the cell was measured with capacitance manometers (MKS Baratron). Samples were excited by a Lambda Physik FL 3002 dye laser (425 nm) and a COMPEX102 excimer laser (308 nm, pulse width 28 ns).

Transient Absorption. The time profiles of the triplet state decay were recorded at 460−500 nm using a 150 W Xe lamp (Phillips) equipped with a pulse unit and a R928 photomultiplier (Hamamatsu) using a laser kinetic spectrometer LKS 20 (Applied Photophysics, UK).

Phosphorescence of $O_2(^1\Delta_g)$ and SODF. Time-resolved near-infrared phosphorescence of $O_2(^1\Delta_g)$ at 1270 nm was observed at a right angle to the excitation pulse using a homemade detector unit (interference filter, Ge diode Judson J16-8SP-R05M-HS). All measurements were performed in an air atmosphere or in air-saturated solutions. The incident energy was within the energy region where the intensity of a phosphorescence signal is directly proportional to the incident energy (less than 1 mJ). Singlet oxygen-sensitized delayed fluorescence (SODF) was monitored at 650 nm (the maximum of the monomer fluorescence emission band) on the laser kinetic spectrometer LKS 20 (Applied Photophysics). The

dx.doi.org/10.1021/jp5029917 | J. Phys. Chem. B 2014, 118, 6167−6174

signals of both SODF and $O_2(^1\Delta_g)$ were averaged from 20–500 traces, and they were calculated as the differences between signals in an air atmosphere or air-saturated solution and the detector responses in a vacuum or argon-saturated solution. The initial part of the signals fails due to light scattering and strong prompt fluorescence of porphyrin, and they were omitted in all figures.

Oxygen Plasma Treatment. PS nanofiber materials for antibacterial tests were oxidized in a radio frequency oxygen plasma (8 W, 30 s, 30 Pa, low pressure FEMTO plasma system from Diener electronic GmbH & Co. KG) to achieve hydrophilic surface properties.

Antibacterial Tests. A culture of *Escherichia coli* (K-12) was incubated with stirring in an LB medium at 37 °C. Incubation was stopped when the absorbance at 560 nm reached a value ca. 1. Then, the culture was diluted by a factor of 2000 to the desired concentration in PBS. The PS nanofiber materials with encapsulated TPP and treated with cold plasma were placed on bacterial agar plates at 5, 25 and 32 °C. The surfaces of the materials were inoculated with 60 μL (ca. 6000 CFU) of a suspension of *Escherichia coli* in PBS. The agar plates were either irradiated with white light from a 400 W solar daylight simulator (Sol1A Newport, USA) with a water filter (for elimination of IR radiation) for 10, 15, or 20 min or stored in the dark 5, 25 and 32 °C. Then the samples of materials were placed in Eppendorf tubes with 1 mL of PBS. After a brief agitation (2 × 3s on IKA Vortex 3), the nanofiber material was removed. The bacterial suspension was centrifuged for 10 min at 3600*g* (7000 rpm), and the supernatant (0.7 mL) was carefully removed. One hundred microliters of bacterial suspensions from pellet media was put on the sterile agar plates. The plates were incubated for 15 h in darkness at 37 °C to allow the individual bacteria to grow and form colonies.

RESULTS AND DISCUSSION

PS Nanofiber Material with TPP Encapsulated Inside Nanofibers. *Morphology and Optical Properties.* The structure of the electrospun PS nanofiber materials with encapsulated TPP was visualized by SEM (Figure 2a). The average diameter of individual nanofibers was ~200 nm. All materials can be activated by a blue light (Soret band in absorption spectrum). Weak absorption can also be found between 500 and 650 nm (four Q-bands). No significant broadening or shift of the bands, which is typical for aggregation of porphyrins, was observed (Figure 2b). Aggregation of porphyrins usually decreases the quantum yield of $O_2(^1\Delta_g)$ (Φ_Δ).[21]

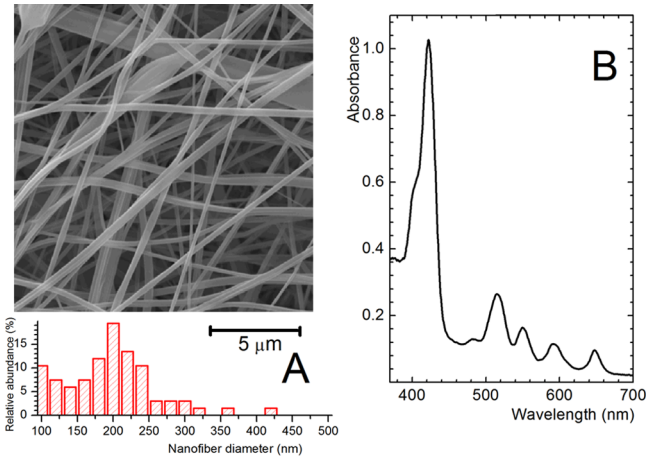

Figure 2. SEM micrograph with the corresponding diameter distributions (panel A) and UV/vis absorption spectrum (panel B) of the PS nanofiber material with encapsulated TPP (1 wt %).

Photogeneration of Porphyrin Triplet States and $O_2(^1\Delta_g)$ in an Air Atmosphere. The kinetics of both TPP triplet states and oxygen $O_2(^1\Delta_g)$ can be described using eqs 1 and 2:[8]

$$[^3\mathrm{TPP}] = [^3\mathrm{TPP}]_0 \exp(-t/\tau_T) \quad (1)$$

$$[O_2(^1\Delta_g)] = A_{SO}\frac{\tau_\Delta}{\tau_T - \tau_\Delta}(\exp(-t/\tau_T) - \exp(-t/\tau_\Delta)) \quad (2)$$

where A_{SO} is a parameter, τ_T is the lifetime of the porphyrin triplet states in air atmosphere, τ_Δ is the corresponding lifetime of $O_2(^1\Delta_g)$, $[O_2(^1\Delta_g)]$ denotes the concentration of $O_2(^1\Delta_g)$ in time t and $[^3\mathrm{TPP}]_0$ and $[^3\mathrm{TPP}]$ are the initial concentrations of the triplet states at time t_0 (immediately after the excitation and intersystem crossing) and at time t, respectively.

We found that the kinetics of both porphyrin triplet states and $O_2(^1\Delta_g)$ are dependent on temperature. Figure 3 shows

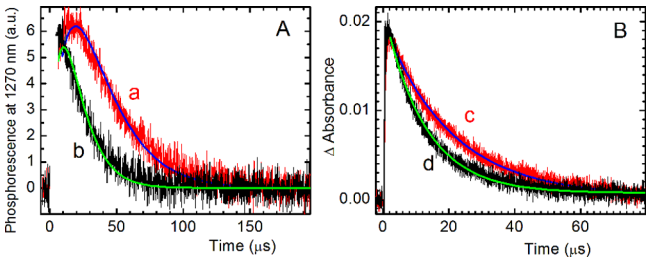

Figure 3. (A) PS nanofiber material with encapsulated TPP in the air atmosphere: Kinetics of $O_2(^1\Delta_g)$ formation and decay at 5 (a) and 55 (b) °C fit by a double exponential function (eq 2), average of 200 traces. (B) Corresponding kinetics of the decay of the TPP triplet states at 5 (c) and 55 (d) °C fit by a single exponential function (eq 1), average of 50 traces.

kinetics of $O_2(^1\Delta_g)$ formation and decay at 5 (a) and 55 (b) °C in PS nanofibers with encapsulated TPP and corresponding kinetics of the decay of the TPP triplet states at 5 (c) and 55 (d) °C measured with the same sample.

The fits using eqs 1 and 2 provided τ_T = 19.6 μs, A_T = 0.020 for 5 °C and τ_T = 11.9 μs, A_T = 0.021 for 55 °C. The corresponding data for $O_2(^1\Delta_g)$ are τ_Δ = 21.7 μs, A_{SO} =17 (5 °C) and τ_Δ = 10.4 μs, A_{SO} = 14 (55 °C) The room temperature lifetimes we report are consistent with data published in a previous paper.[22] Each value of τ_T and τ_Δ at different temperatures represents an average of at least three independent measurements.

The amplitudes of both TPP triplet states and $O_2(^1\Delta_g)$ kinetics were nearly independent with respect to temperature (Figure 3 and Supporting Information). These results indicate that quantum yield of the triplet states (Φ_T) and $O_2(^1\Delta_g)$ (Φ_Δ) did not change significantly in temperature range between 5–55 °C. The heterogeneity of the materials did not allow exact calculation of both Φ_T and Φ_Δ. The deviations of $O_2(^1\Delta_g)$ kinetics from the expected results (eq 2) at the early stages of $O_2(^1\Delta_g)$ kinetics are due to singlet oxygen-sensitized delayed fluorescence, which is discussed below.

We have also tested the influence of heterogeneity of nanofiber materials (different nanofiber diameter, presence of

dx.doi.org/10.1021/jp5029917 | J. Phys. Chem. B 2014, 118, 6167–6174

nodes, difference in distribution of porphyrin molecules inside nanofibers, etc.) on the kinetics of $O_2(^1\Delta_g)$. The measurements were performed at room temperature (25 °C) with several samples (~1 cm^2) from different places of nanofiber material with an original size of ~2 × 1 m. The fitting procedure (eq 2) with fixed τ_T = 16 μs (calculated from transient absorption measurements) gave τ_Δ = 15.7 ± 0.5 μs, which is an average of over 15 samples.

Four cycles of heating up to 60 °C followed by cooling down to 5 °C did not induce any observable changes in the photophysical properties (amplitudes and lifetimes of the TPP triplet states and $O_2(^1\Delta_g)$) at the selected temperature. It indicates that the temperature-controlled photophysical properties of PS nanofiber materials with encapsulated TPP are reversible.

A dominant channel for the TPP triplet states deactivation is through quenching by oxygen with a rate constant of k_q [O_2]. Because the solubility of diatomic gases in the condensed phase or polymers is only weakly dependent on temperature,[23] we neglect temperature effects on the concentration of oxygen in the ground state dissolved in a polymer. The values of $1/\tau_T = k_q$ [O_2] (eq 3) were then examined using an Arrhenius treatment (Figure 4, panel A):

$$1/\tau_T = A \exp(-E_a/RT) \quad (3)$$

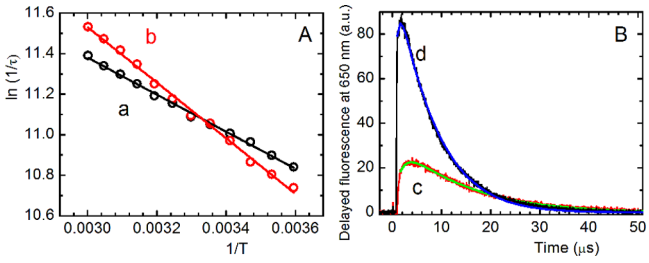

Figure 4. Arrhenius plot for decay of TPP triplet states (a) and $O_2(^1\Delta_g)$ (b) in PS nanofiber material with encapsulated TPP (1 wt %) in an air atmosphere. The solid lines are linear fits to the data (panel A). Corresponding kinetics of SODF calculated as the difference in the fluorescence at 650 nm in an air (prompt fluorescence and SODF) and argon (only prompt fluorescence) atmosphere at 5 (c) and 55 (d) °C fit by eq 7 (panel B, average of five traces).

It is known that the quenching of TPP triplet states by oxygen occurs at or near the diffusion-controlled limit in the polymer. The corresponding quenching constant $k_q = \alpha k_{diff}$ can be expressed by eq 4:[22,23]

$$k_q = \frac{4\pi\alpha N_A \sigma}{1000} D(O_2) \quad (4)$$

where α is the probability of quenching in the encounter complex; k_{diff} is the diffusion controlled rate constant; N_A is Avogadro's number; $D(O_2)$ is the diffusion coefficient for oxygen in the polymer; and σ is the collision diameter of the ^{3}TPP−O_2 complex.

If α is constant and independent of temperature, we can assume that the activation energy for the quenching of TPP by oxygen is equal to the activation energy for oxygen diffusion (see eq 5, which is a combination of eqs 3 and 4):

$$D(O_2) = \frac{1000A}{4\pi N_A \sigma \alpha [O_2]} \exp(-E_a/RT) \quad (5)$$

The calculated value of apparent activation energy, E_a, calculated from eq 3 was 7.6 ± 0.2 kJ mol^{-1} (Figure 4a) and corresponds with temperature changes in the diffusion of O_2 in the ground state to TPP triplet states. The literature value for the activation barrier for oxygen diffusion through thick (~30 μm) PS film is 4 times higher (~30 kJ mol^{-1}).[19] The reason for this difference may be the low diameters of the PS nanofiber and the nonhomogeneous character of the material. Contributions from solids, the solid−gas interface, and the gas phase can be expected, all having different activation parameters. The diffusion of O_2 in our measurements also occurs along very short distances due to presence of dissolved O_2 inside the polymers under the air atmosphere. The distance between TPP molecules (~5 nm for PS nanofiber material with 1 wt % encapsulated TPP)[24] is comparable with the size of TPP molecule and the collision diameter σ of the ^{3}TPP−O_2 complex.

The main deactivation channel of $O_2(^1\Delta_g)$ is a nonradiative interaction with its environment. The contribution of phosphorescence at 1270 nm used for monitoring $O_2(^1\Delta_g)$ for its deactivation rate constant is negligible.[25] Recently, the temperature effect on lifetimes of $O_2(^1\Delta_g)$ in different liquid solvents was evaluated[18,26] and it was found that lifetimes of $O_2(^1\Delta_g)$ are controlled by diffusion with a solvent-dependent apparent activation energy, E_a'. Consistently, a similar Arrhenius treatment was also applied to deactivation of $O_2(^1\Delta_g)$ in PS nanofiber materials with encapsulated TPP (eq 6):

$$1/\tau_\Delta = A' \exp(-E_a'/RT) \quad (6)$$

The apparent activation energy E_a' for the deactivation of $O_2(^1\Delta_g)$ in PS nanofiber materials is 11.4 ± 0.2 kJ mol^{-1} (Figure 4b), and it is higher than the corresponding data for deactivation in liquid solvents.[18]

SODF. The deviation from the kinetics of $O_2(^1\Delta_g)$ in early stages after excitation (see, e.g., Figure 3) is due to energy losses by SODF. A strong SODF signal occurs from the reaction of triplet porphyrin photosensitizers with $O_2(^1\Delta_g)$ (Figure 1). Other mechanisms of delayed fluorescence, notably triplet−triplet annihilation and thermally activated reverse intersystem crossing, were excluded because no signal of delayed fluorescence was detected in a vacuum or argon atmosphere.[24]

For a more quantitative description of SODF kinetics, we used a homogeneous kinetic model similar to those used previously,[27] which was described in detail in our previous paper.[24] This simple model does not include heterogeneity of the material and the contribution of $O_2(^1\Delta_g)$ diffusing outside of the nanofibers, because SODF only arises inside nanofibers. The SODF traces at different temperatures were fit by eq 7, which was derived from differential equations using a detailed kinetic scheme (Figure 1):

$$I_{SODF} = A'_{SODF} \exp\left\{-\frac{t}{\tau_T} + k_q^1 \tau_T [^3TPP]_0 \exp\left(-\frac{t}{\tau_T}\right)\right\} \sum_{n=0}^{\infty} (-k_q^1 [^3TPP]_0 \tau_T)^n \frac{\exp\left[-\frac{(n+1)t}{\tau_T}\right] - \exp\left(\frac{1}{\tau_\Delta}\right)}{\left(\frac{1}{\tau_\Delta} - \frac{n+1}{\tau_T}\right) n!} \quad (7)$$

The parameters of the fit were amplitude A'_{SODF}, τ_Δ, and the product $k_q^1[^3TPP]_0$; whereas, τ_T was obtained by the

dx.doi.org/10.1021/jp5029917 | J. Phys. Chem. B 2014, 118, 6167−6174

monoexponential analysis of the TPP triplet states measured by transient absorption spectroscopy (Figure 3, panel B).

We previously tested this model on polyurethane Larithan nanofiber materials with more effective quenching of TPP triplet states.[24] The value of τ_T in an air atmosphere at room temperature was approximately 2 times lower than the value for the PS nanofiber materials. The fitting procedures provided reasonable values of τ_Δ and τ_T, which are comparable to those obtained from phosphorescence and transient absorption measurements. The results for PS nanofiber materials show deviations from the model (A'_{SODF} = 0.4, τ_Δ = 5.1 μs at 5 °C and A'_{SODF} = 2.2, τ_Δ = 1.5 μs at 55 °C; Figure 4c,d). The values of τ_Δ calculated from SODF traces (eq 7) for PS nanofiber materials are significantly lower than the values calculated from direct phosphorescence measurements at 1270 nm (eq 2).

The increase in SODF intensity with increasing temperature (Figure 4, panel B) and the 5-fold increase of amplitude, A'_{SODF}, between temperatures 5 and 55 °C (eq 7) are consistent with previous results, and it is due to increased diffusion of $O_2(^1\Delta_g)$ to the TPP triplet states in nanofiber materials. We conclude that SODF is a very sensitive method of detection of $O_2(^1\Delta_g)$ inside polymers or polymeric nanofibers because direct phosphorescence measurements require the averaging of more traces to achieve a comparable S/N ratio. However, calculating τ_Δ and τ_T using a simple model (eq 7) for heterogeneous nanofiber materials may provide different values than the results of phosphorescence or transient absorption measurements.

Influence of Polymeric Matrices. We also tested two polyurethanes, Larithane and medical-grade Tecophilic nanofiber materials, with encapsulated TPP (1 wt %). These had been studied in a previous paper at room temperature (Figure 5).[22]

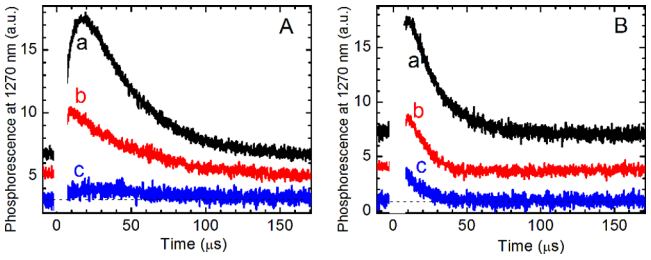

Figure 5. Kinetics of $O_2(^1\Delta_g)$ formation and decay in PS (a), polyurethanes Larithane (b), and Tecophilic (c) nanofiber materials with encapsulated TPP (1 wt %) in an air atmosphere at 5 (panel A) and 55 (panel B) °C.

The changes in the amplitudes and lifetimes of $O_2(^1\Delta_g)$ with temperature are higher for both polyurethanes in comparison with PS. The differences may correspond to a differing solubility of oxygen in polyurethanes or to the structure of polymers (number of quenching sites for $O_2(^1\Delta_g)$). Other contributions may include the temperature-responsive dynamic behavior of the individual nanofiber materials, e.g., (irreversible) thermal shrinkage of nanofibers.[28,29] The photophysical properties may also be influenced by the swelling of nanofibers due to humidity, e.g., Tecophilic absorbs equilibrium water contents of up to 150% of the weight of dry nanofibers.[30]

The heterogeneity of nanofiber materials and irreversibility of some processes due to heating do not allow a comparison of the efficiency of $O_2(^1\Delta_g)$ photogeneration between individual polymers simply on the basis of amplitudes of corresponding phosphorescence signals. Nevertheless, we identified PS nanofiber material as having efficient photooxidation at temperatures ranging between 5 and 55 °C due to the relatively efficient production of $O_2(^1\Delta_g)$ with a low activation barrier and temperature reversibility.

Influence of Aqueous Environment. Diffusion of $O_2(^1\Delta_g)$ outside nanofibers is necessary for the successful application of nanofiber materials. The properties of the nanofibers environment influences the decay of $O_2(^1\Delta_g)$. Figure 6 shows the kinetics of $O_2(^1\Delta_g)$ in PS nanofiber materials immersed in D_2O (panel A) and H_2O (panel B) in the temperature range between 5 and 55 °C.

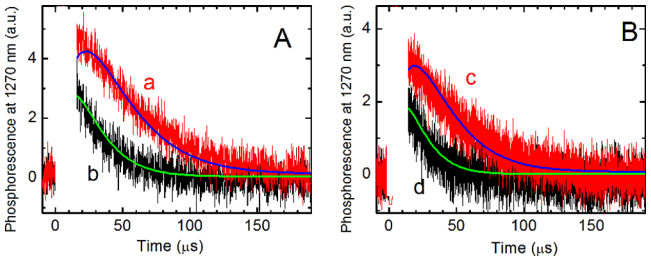

Figure 6. Kinetics of $O_2(^1\Delta_g)$ formation and decay of PS nanofiber material with encapsulated TPP at 5 (a) and 55 (b) °C in D_2O (panel A) and corresponding kinetics at 5 (c) and 55 (d) °C in H_2O (panel B).

In order to fit the $O_2(^1\Delta_g)$ traces (Figure 6), the lifetime τ_T was fixed and was taken from previous experiments in the air atmosphere, because encapsulated porphyrin molecules are not in direct contact with nanofiber environment. The calculated values of τ_Δ changed from 26.7 μs at 5 °C to 17.2 μs at 55 °C for the D_2O environment and from 23.8 μs at 5 °C to 10.7 μs at 55 °C for the H_2O environment. These results show a higher quenching effect of H_2O in this temperature range.

PS Nanofiber Material with Externally Bound Porphyrin in Aqueous Solution. A critical aspect of materials with a photosensitizer immobilized inside fibers is the diffusion length of $O_2(^1\Delta_g)$ (typically tens to hundreds of nanometers in both polymer matrices and aqueous solutions),[24] which limits photooxidation processes to areas in close proximity to the nanofiber surfaces. Thus, higher photooxidation efficiency requires the organization of photosensitizer molecules near nanofiber surfaces, which is not easy to control,[31] or external binding of the photosensitizer to the surface of the nanofibers.

In our previous study,[10] we prepared nanofiber materials with externally bound 5,10,15,20-tetrakis(1-methylpyridinium-4-yl)-porphyrin photosensitizer (TMPyP), which is photoactive in aqueous medium and generates $O_2(^1\Delta_g)$ after irradiation with a high quantum yield (Φ_Δ= 0.74 for homogeneous solution of TMPyP in water).[32] The combination of the electrospinning technique and electrostatic assembly allows us to take advantage of the highly specific surface area, easy exposure of the porphyrin molecules to light and oxygen, flexibility, light weight, and high porosity of the nanofiber materials. This type of nanofiber material is less photoactive in the dry state, possibly due to surface changes and aggregation of the photosensitizer.

Figure 7, panel A, demonstrates a weak dependence of $O_2(^1\Delta_g)$ kinetics on temperature for photogeneration by TMPyP externally bound to PS nanofiber materials immersed in H_2O. This is consistent with the results for the temperature

dx.doi.org/10.1021/jp5029917 | J. Phys. Chem. B 2014, 118, 6167−6174

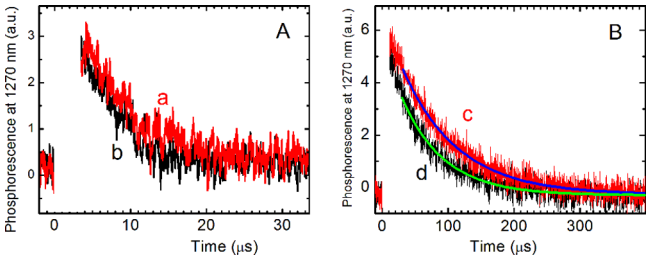

Figure 7. Kinetics of $O_2(^1\Delta g)$ formation and decay in PS nanofiber materials with externally bound TMPyP at 5 (a) and 55 (b) °C in H_2O (panel A) and at 5 (c) and 55 (d) °C in D_2O (panel B).

dependence of $O_2(^1\Delta_g)$ in pure H_2O, which has a low apparent activation energy of 1.2 kJ mol^{-1}.[18] Taking into account that the lifetime of $O_2(^1\Delta_g)$ in H_2O is ~3.5 μs,[33] and the lifetime of the triplet states of adsorbed TMPyP was found to be ~8 μs at room temperature,[10] it is clear that the $O_2(^1\Delta_g)$ kinetics match the kinetics of the TMPyP triplet states, and $O_2(^1\Delta_g)$ is efficiently deactivated by collisions with water molecules.

We also performed measurements in D_2O, where the lifetime of $O_2(^1\Delta_g)$ is ~20 times higher than in H_2O. First, we recalculate the apparent activation energy for the deactivation of $O_2(^1\Delta_g)$ in pure D_2O. Singlet oxygen $O_2(^1\Delta_g)$ was generated by the water-soluble porphyrin derivative TPPS, and measurements were performed in the temperature range between 5 and 55 °C (Figure 8a,b). We used a similar treatment to the one

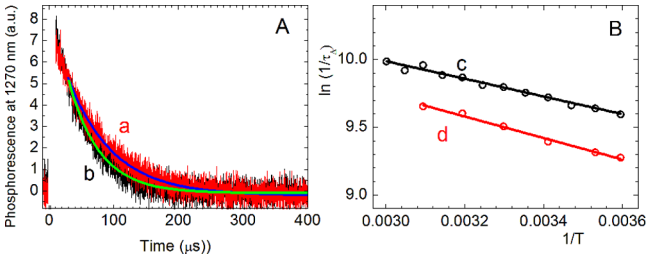

Figure 8. Kinetics of $O_2(^1\Delta g)$ generated by TPPS in D_2O solution at 5 (a) and 55 (b) °C. The solid lines are single-exponential fits to the data (panel A). Arrhenius plots for deactivation of $O_2(^1\Delta_g)$ formed from irradiation of TPPS in D_2O (c) and from TMPyP bound on PS nanofiber materials immersed in D_2O (d). The solid lines are linear fits to the data (panel B).

described above (eq 6), which yielded an apparent activation energy $E_a' = 5.4 \pm 0.3$ kJ mol^{-1} (Figure 8c) that is consistent with the value published in literature.[18]

A significant stabilization effect of PS nanofiber materials on the lifetime of $O_2(^1\Delta g)$ was found. The calculated values of τ_Δ for porphyrin (TPPS) in pure D_2O were 69.3 μs at 5 °C (Figure 8a) and 48.3 μs at 50 °C (Figure 8b). The corresponding values for porphyrin (TMPyP) bound on PS nanofiber materials immersed in D_2O were 93.6 μs at 5 °C (Figure 7c) and 64.1 μs at 50 °C (Figure 7d)). These results are surprising; they may correspond to the diffusion of $O_2(^1\Delta g)$ into the bulk polymer with a low number of possible quenching sites, because SODF does not occur inside nanofibers due to absence of porphyrin triplet states. The sulfate groups at solid–liquid interface between nanofibers and D_2O or hydrogen–deuterium isotope exchange[34] may also contributed to stabilization of $O_2(^1\Delta_g)$.

The Arrhenius plot (eq 6) gave $E_a' = 6.6 \pm 0.3$ kJ mol^{-1} (Figure 8d). This value is comparable with the value in pure D_2O (5.4 ± 0.3 kJ mol^{-1}, Figure 8c) and lower than the values measured for $O_2(^1\Delta g)$ generated inside nanofibers (11.4 ± 0.2 kJ mol^{-1}, Figure 4b), with diffusion coefficients approximately 2 orders of magnitude lower than those in aqueous solution.

Despite the fact that nanofiber material with externally bound porphyrin generates $O_2(^1\Delta_g)$ with lower lifetimes than previously reported nanofiber materials with porphyrin encapsulated inside the PS nanofibers, both materials exhibited high photooxidation activity in aqueous media.[10] A possible reason is longer diffusion length of $O_2(^1\Delta_g)$ from encapsulated porphyrin molecules to the target molecule/structure, whereas externally bound porphyrin photogenerated $O_2(^1\Delta_g)$ in close proximity of the target.

Antibacterial Properties of Nanofiber Materials at Different Temperatures. The light-induced antibacterial properties of the nanofiber material with externally bound TMPyP on bacterial strains of *Escherichia coli* were confirmed and discussed in our previous study.[10] In contrast, the antibacterial properties of hydrophobic PS nanofibers with encapsulated TPP photosensitizers are low. These results are not surprising because the diffusion diameter for $O_2(^1\Delta g)$ in aqueous medium (tens to hundreds of nm)[30] requires close contact between nanofiber surfaces and bacteria. To improve the adhesion of bacteria, we used postprocessing of pristine nanofiber surfaces by oxygen plasma. The effect of plasma processing on temperature dependent behavior of nanofiber materials is negligible (Supporting Information, Figure S7).

The most accepted mechanisms for antibacterial activity under light irradiation are via damage to the cell membrane and alteration to the cell morphology due to light-generated unstable species, especially $O_2(^1\Delta_g)$.[35] The complexity and the density of the cell wall of the microorganisms play a key role in their resistance to antibacterial treatment.[36] In this mechanism, the light-induced antibacterial properties of nanofiber materials with encapsulated TPP are controlled by the diffusion of $O_2(^1\Delta_g)$ toward bacteria and its reactivity with target species.[37]

The antibacterial properties were tested at 32 °C (human skin temperature), 25 °C (room temperature) and 5 °C. The low temperature limit for *Escherichia coli* growth is 7.5 °C (ref 38) but the bacteria can survive at 5 °C (ref 39). Figure 9A–D shows examples of bacterial colonies on agar plates after inoculation with *Escherichia coli* from the surface of PS nanofiber materials with and without encapsulated TPP photosensitizers at 5 and 32 °C before and after irradiation. Agar plates using inoculum on PS nanofiber materials with encapsulated TPP kept in the dark were also used as negative controls. The antibacterial activity decreases with decreasing temperature (Figure 9E). This difference is probably even higher. It was influenced by the condensation of water (evaporated from the sample at 32 °C) on the cover of Petri dish, which serves as a window for irradiation, and therefore, reduces the intensity of incident light. Obviously, these results are also influenced by differences in cell proliferation and nutrient uptake at different temperatures.

A stronger antibacterial effect at higher temperature (Figure 9) is consistent with photophysical measurements (see above) where we found that the diffusion coefficient of oxygen increased with increasing temperature in polymeric nanofibers.

■ CONCLUSIONS

This paper presents results of the systematic investigation of $O_2(^1\Delta_g)$ and the porphyrin triplet state kinetics generated by

dx.doi.org/10.1021/jp5029917 | J. Phys. Chem. B 2014, 118, 6167–6174

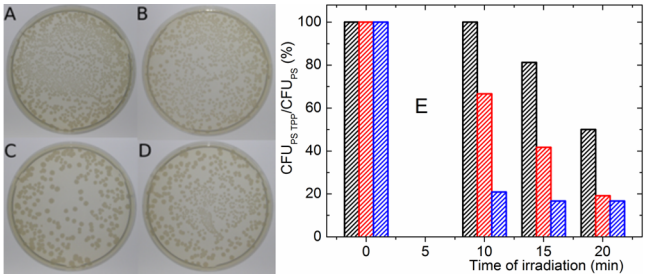

Figure 9. Colonies of *Escherichia coli* on agar plates after inoculation from the surface of plasma treated PS nanofiber materials without photosensitizer at 32 °C (A) and at 5 °C (B) and material with encapsulated TPP at 32 °C (C) and at 5 °C (D) after 20 min of irradiation and 18 h of incubation. Photoantibacterial activity of plasma treated PS nanofiber material with encapsulated TPP (E) was estimated as a proportion of CFU of *Escherichia coli* found on agar plates after inoculation from the surface of samples without photosensitizer compared with a TPP photosensitizer irradiated for 0, 10, 15, and 20 min at 5 °C (black), 25 °C (red) and 32 °C (blue) and incubated for 18 h. Irradiation was performed by a 400 W solar simulator equipped with a water filter.

the irradiation of porphyrin photosensitizers inside and outside of polymeric nanofiber materials as a function of temperature. It provides insight into a potential application of photoactive nanofiber materials at different temperatures. An increase in temperature led to an increase in diffusion of the $O_2(^1\Delta_g)$ and oxygen in the ground state toward quenchers (quenching groups, porphyrin triplets) and a corresponding shortening its lifetime but did not significantly influence the yield of $O_2(^1\Delta_g)$ formation. Nanofiber materials with externally bound porphyrin have a considerably weaker temperature dependence for $O_2(^1\Delta_g)$ lifetimes than polymeric nanofiber materials with encapsulated porphyrin.

The diffusion of $O_2(^1\Delta_g)$ toward bacteria control the antibacterial properties of PS nanofiber materials with encapsulated TPP. These properties increase at higher temperature. The significant effect in antibacterial treatment plays also the adhesion of bacteria to the nanofiber surface. Further studies are under progress to investigate the influence of nanofiber surface modifications on antibacterial properties. SODF is a very sensitive method for sensing of $O_2(^1\Delta_g)$ in trace concentrations inside polymeric objects; however, the exact calculation of lifetimes of the porphyrin triplet states and $O_2(^1\Delta_g)$ may provide different values than phosphorescence and transient absorption measurements. A significant increase in SODF at high temperature corresponds with higher diffusion of $O_2(^1\Delta_g)$ toward triplet porphyrin molecules in the polymer matrix.

■ ASSOCIATED CONTENT

Supporting Information

Temperature-dependent phosphorescence of $O_2(^1\Delta g)$, kinetics of porphyrin triplet states and SODF of different nanofiber materials and in different media, calculated lifetimes of the porphyrin triplet states and $O_2(^1\Delta_g)$. This material is available free of charge via the Internet at http://pubs.acs.org.

■ AUTHOR INFORMATION

Corresponding Author

*E-mail address: pavel.kubat@jh-inst.cas.cz.

Notes

The authors declare no competing financial interest.

■ ACKNOWLEDGMENTS

This research was supported by the Czech Science Foundation (Grant No. 13-12496S). The authors thank Lukáš Plíštil (Faculty of Sciences, Charles University in Prague) for preparing the nanofiber materials using the electrospinning technique, Jitka Forstová (Faculty of Sciences, Charles University in Prague) for her help with antibacterial tests and Anna Artemenko (Institute of Physics, Academy of Sciences of the Czech Republic) for modification of PS nanofiber materials by oxygen plasma.

■ ABBREVIATIONS

TPP, 5,10,15,20-tetraphenylporphyrin; TMPyP, 5,10,15,20-tetrakis(1-methylpyridinium-4-yl) porphyrin tetra(*p*-toluenesulfonate); TPPS, 10,15,20-tetrakis(4-sulfonatophenyl)porphyrin tetrasodium salt; TEAB, tetraethylamonium bromide; SODF, singlet oxygen-sensitized delayed fluorescence; PS, polystyrene; Φ_Δ, quantum yield of $O_2(^1\Delta_g)$; CFU, colony forming unit

■ REFERENCES

(1) Ogilby, P. R. Singlet Oxygen: There is Indeed Something New Under the Sun. *Chem. Soc. Rev.* **2010**, *39*, 3181−3209.
(2) Dougherty, T. J.; Gomer, C. J.; Henderson, B. W.; Jori, G.; Kessel, D.; Korbelik, M.; Moan, J.; Peng, Q. Photodynamic Therapy. *J. Nat. Cancer Inst.* **1998**, *90*, 889−905.
(3) Maisch, T.; Baier, J.; Franz, B.; Maier, M.; Landthaler, M.; Szeimies, R. M.; Baumler, W. The Role of Singlet Oxygen and Oxygen Concentration in Photodynamic Inactivation of Bacteria. *Proc. Natl. Acad. Sci. U. S. A.* **2007**, *104*, 7223−7228.
(4) Strassert, C. A.; Otter, M.; Albuquerque, R. Q.; Höne, A.; Vida, Y.; Maier, B.; De Cola, L. Photoactive Hybrid Nanomaterial for Targeting, Labeling, and Killing Antibiotic-Resistant Bacteria13. *Angew. Chem., Int. Ed.* **2009**, *48*, 7928−7931.
(5) Xing, C.; Yang, G.; Liu, L.; Yang, Q.; Lv, F.; Wang, S. Conjugated Polymers for Light-Activated Antifungal Activity. *Small* **2012**, *8*, 525−529.
(6) Arzoumanian, E.; Ronzani, F.; Trivella, A.; Oliveros, E.; Sarakha, M.; Richard, C.; Blanc, S.; Pigot, T.; Lacombe, S. Transparent Organosilica Photocatalysts Activated by Visible Light: Photophysical and Oxidative Properties at the Gas−Solid Interface. *ACS Appl. Mater. Interfaces* **2014**, *6*, 275−288.
(7) Aebisher, D.; Azar, N. S.; Zamadar, M.; Gandra, N.; Gafney, H. D.; Gao, R.; Greer, A. Singlet Oxygen Chemistry in Water: A Porous Vycor GlassSupported Photosensitizer. *J. Phys. Chem. B* **2008**, *112*, 1913−1917.
(8) Mosinger, J.; Jirsák, O.; Kubát, P.; Lang, K.; Mosinger, B. Bactericidal Nanofabrics Based on Photoproduction of Singlet Oxygen. *J. Mater. Chem.* **2007**, *17*, 164−166.
(9) Mosinger, J.; Lang, K.; Kubát, P.; Sýkora, J.; Hof, M.; Plíštil, L.; Mosinger, B., Jr Photofunctional Polyurethane Nanofabrics Doped by Zinc Tetraphenylporphyrin and Zinc Phthalocyanine Photosensitizers. *J. Fluoresc.* **2009**, *19*, 705−713.
(10) Henke, P.; Lang, K.; Kubát, P.; Sýkora, J.; Šlouf, M.; Mosinger, J. Polystyrene Nanofiber Materials Modified with an Externally Bound Porphyrin Photosensitizer. *ACS Appl. Mater. Interfaces* **2013**, *5*, 3776−3783.
(11) Greiner, A.; Wendorff, J. H. Electrospinning: A Fascinating Method for the Preparation of Ultrathin Fibres. *Angew. Chem., Int. Ed.* **2007**, *46*, 5670−5703.
(12) Pitsillides, C. M.; Joe, E. K.; Wei, X.; Anderson, R. R.; Lin, C. P. Selective Cell Targeting with Light-Absorbing Microparticles and Nanoparticles. *Biophys. J.* **2003**, *84*, 4023−4032.

(13) Gracanin, M.; Hawkins, C. L.; Pattison, D. I.; Davies, M. J. Singlet-Oxygen-Mediated Amino Acid and Protein Oxidation: Formation of Tryptophan Peroxides and Decomposition Products. *Free Radical Biol. Med.* **2009**, *47*, 92−102.
(14) Botes, M.; Eugene Cloete, T. The Potential of Nanofibers and Nanobiocides in Water Purification. *Crit. Rev. Microbiol.* **2010**, *36*, 68−81.
(15) Arenbergerova, M.; Arenberger, P.; Bednar, M.; Kubat, P.; Mosinger, J. Light-Activated Nanofibre Textiles Exert Antibacterial Effects in the Setting of Chronic Wound Healing. *Exp. Dermatol.* **2012**, *21*, 619−624.
(16) Bower, J. P.; Anastasio, C. Using Singlet Molecular Oxygen to Probe the Solute and Temperature Dependence of Liquid-Like Regions in/on Ice. *J. Phys. Chem. A* **2013**, *117*, 6612−6621.
(17) Bower, J. P.; Anastasio, C. Measuring a 10,000-fold Enhancement of Singlet Molecular Oxygen ($^1O_2$*) Concentration on Illuminated Ice Relative to the Corresponding Liquid Solution. *Atmos. Environ.* **2013**, *75*, 188−195.
(18) Jensen, R. L.; Arnbjerg, J.; Ogilby, P. R. Temperature Effects on the Solvent-Dependent Deactivation of Singlet Oxygen. *J. Am. Chem. Soc.* **2010**, *132*, 8098−8105.
(19) Gao, Y.; Baca, A. M.; Wang, B.; Ogilby, P. R. Activation Barriers for Oxygen Diffusion in Polystyrene and Polycarbonate Glasses: Effects of Low Molecular Weight Additives. *Macromolecules* **1994**, *27*, 7041−7048.
(20) Recknor, J. B.; Recknor, J. C.; Sakaguchi, D. S.; Mallapragada, S. K. Oriented Astroglial Cell Growth on Micropatterned Polystyrene Substrates. *Biomaterials* **2004**, *25*, 2753−2767.
(21) Procházková, K.; Zelinger, Z.; Lang, K.; Kubát, P. Meso-Tetratolylporphyrins Substituted by Pyridinium Groups: Aggregation, Photophysical Properties and Complexation with DNA. *J. Phys. Org. Chem.* **2004**, *17*, 890−897.
(22) Jesenská, S.; Plíštil, L.; Kubát, P.; Lang, K.; Brožová, L.; Popelka, Š.; Szatmáry, L.; Mosinger, J. Antibacterial Nanofiber Materials Activated by Light. *J. Biomed. Mater. Res., Part A* **2011**, *99A*, 676−683.
(23) Lu, X.; Winnik, M. A. Luminescence Quenching in Polymer/Filler Nanocomposite Films Used in Oxygen Sensors. *Chem. Mater.* **2001**, *13*, 3449−3463.
(24) Mosinger, J.; Lang, K.; Plístil, L.; Jesenská, S.; Hostomský, J.; Zelinger, Z.; Kubát, P. Fluorescent Polyurethane Nanofabrics: A Source of Singlet Oxygen and Oxygen Sensing. *Langmuir* **2010**, *26*, 10050−10056.
(25) Schweitzer, C.; Schmidt, R. Physical Mechanisms of Generation and Deactivation of Singlet Oxygen. *Chem. Rev.* **2003**, *103*, 1685−1758.
(26) Jensen, R. L.; Holmegaard, L.; Ogilby, P. R. Temperature Effect on Radiative Lifetimes: The Case of Singlet Oxygen in Liquid Solvents. *J. Phys. Chem. B* **2013**, *117*, 16227−16235.
(27) Levin, P. P.; Costa, S. M. B.; Ferreira, L. F. V.; Lopes, J. M.; Ribeiro, F. R. Delayed Fluorescence Induced by Molecular Oxygen Quenching of Zinc Tetraphenylporphyrin Triplets at Gas/Solid Interfaces of Silica and Zeolite. *J. Phys. Chem. B* **1997**, *101*, 1355−1363.
(28) Kim, B. K.; Lee, S. Y.; Xu, M. Polyurethanes Having Shape Memory Effects. *Polymer* **1996**, *37*, 5781−5793.
(29) Lin, X.; Tang, D.; Yu, Z.; Feng, Q. Stimuli-Responsive Electrospun Nanofibers from Poly(*N*-isopropylacrylamide)-*co*-poly(acrylic acid) Copolymer and Polyurethane. *J. Mater. Chem. B* **2014**, 651−658.
(30) Mosinger, J.; Lang, K.; Hostomský, J.; Franc, J.; Sýkora, J.; Hof, M.; Kubát, P. Singlet Oxygen Imaging in Polymeric Nanofibers by Delayed Fluorescence. *J. Phys. Chem. B* **2010**, *114* (48), 15773−15779.
(31) Arai, T.; Tanaka, M.; Kawakami, H. Porphyrin-Containing Electrospun Nanofibers: Positional Control of Porphyrin Molecules in Nanofibers and Their Catalytic Application. *ACS Appl. Mater. Interfaces* **2012**, *4* (10), 5453−5457.
(32) Wilkinson, F.; Helman, W. P.; Ross, A. B. Quantum Yields for the Photosensitized Formation of the Lowest Electronically Excited Singlet-State of Molecular Oxygen in Solution. *J. Phys. Chem. Ref. Data* **1993**, *22* (1), 113−262.
(33) Poulsen, T. D.; Ogilby, P. R.; Mikkelsen, K. V. Solvent Effects on the $O_2(a^1\Delta_g)-O_2(X^3\Sigma_g^-)$ Radiative Transition: Comments Regarding Charge-Transfer Interactions. *J. Phys. Chem. A* **1998**, *102* (48), 9829−9832.
(34) Junk, T.; Catallo, W. J. Hydrogen Isotope Exchange Reactions Involving C−H (D, T) Bonds. *Chem. Soc. Rev.* **1997**, *26* (5), 401−406.
(35) Wang, Y.; Jett, S. D.; Crum, J.; Schanze, K. S.; Chi, E. Y.; Whitten, D. G. Understanding the Dark and Light-Enhanced Bactericidal Action of Cationic Conjugated Polyelectrolytes and Oligomers. *Langmuir* **2012**, *29* (2), 781−792.
(36) Tatsuzawa, H.; Maruyama, T.; Misawa, N.; Fujimori, K.; Nakano, M. Quenching of Singlet Oxygen by Carotenoids Produced in *Escherichia coli* − Attenuation of Singlet Oxygen-Mediated Bacterial Killing by Carotenoids. *FEBS Lett.* **2000**, *484* (3), 280−284.
(37) Lissi, E. A.; Encinas, M. V.; Lemp, E.; Rubio, M. A. Singlet Oxygen $O_2(^1\Delta_g)$ Bimolecular Processes. Solvent and Compartmentalization Effects. *Chem. Rev.* **1993**, *93* (2), 699−723.
(38) Strocchi, M.; Ferrer, M.; Timmis, K. N.; Golyshin, P. N. Low Temperature-Induced Systems Failure in *Escherichia coli*: Insights from Rescue by Cold-Adapted Chaperones. *Proteomics* **2006**, *6* (1), 193−206.
(39) Blaustein, R. A.; Pachepsky, Y.; Hill, R. L.; Shelton, D. R.; Whelan, G. *Escherichia coli* Survival in Waters: Temperature Dependence. *Water Res.* **2013**, *47* (2), 569−578.